ORIENTAL JOURNAL OF CHEMISTRY
An International Open Access, Peer Reviewed Research Journal
www.orientjchem.org
ISSN: 0970-020 X
CODEN: OJCHEG
2026, Vol. 42, No.(2):
Pg. 478-492

Development and Characterization of a pH-responsive Cellulose-Gelatin Film Containing Clitoria ternatea Anthocyanin Extract for Intelligent Packaging Application

CRIS G. DE TORRES, SHAIRA MAE G. BENDAÑA, KEN BYRON M. RECEDE, ROSENDA A. BRONCE and REYGAN H. SANGALANG*

College of Arts and Sciences, Batangas State University The National Engineering University, Pablo Borbon Campus, Batangas City, Batangas, Philippines, 4200

*Corresponding author E-mail: reygan.sangalang@g.batstate-u.edu.ph

http://dx.doi.org/10.13005/ojc/420211

(Received: February 10, 2026; Accepted: March 27, 2026)

ABSTRACT

This study developed pH-responsive films composed of cellulose, gelatin, and anthocyanin for potential application as food spoilage indicators in intelligent packaging. Several plant sources of anthocyanin were initially screened for their pH color response, and Clitoria ternatea extract exhibited the most distinct and stable transition at pH ≥ 6, making it suitable for detecting meat spoilage. Cellulose–gelatin–anthocyanin (CGA) films were fabricated with varying anthocyanin concentrations and characterized for their physicochemical, mechanical, and colorimetric properties. Surface morphology analysis showed that moderate anthocyanin incorporation improved film surface uniformity, while higher loading increased surface roughness. Functional group analysis confirmed successful integration of anthocyanin into the cellulose–gelatin matrix. Increasing anthocyanin concentration affected several film properties: opacity increased from 10.04 to 13.31 mm ^{1} and water content from 7.66 ± 0.10% to 10.12 ± 0.21%, while water solubility decreased from 47.99 ± 0.40% to 30.60 ± 0.35%. Mechanical performance improved, with tensile strength increasing from 9.74 MPa to 21.11 MPa and elongation at break from 0.60 ± 0.29% to 1.79 ± 0.20%. The films were thermally stable up to approximately 200 °C and exhibited concentration-dependent color changes when exposed to ammonia vapor (136 ppm), with the 6% anthocyanin film showing the highest color difference (E = 16.43). These results highlight the potential of cellulose–gelatin–anthocyanin films as sustainable indicators in intelligent packaging for real-time food freshness monitoring.

Keywords: Anthocyanins, Cellulose, Clitoria ternatea, Gelatin, Intelligent food packaging, pH-responsive film.

INTRODUCTION

Perishable meat and seafood products are highly susceptible to spoilage due to microbial growth and enzymatic activity during storage. As bacteria decompose proteins and amino acids in fish, pork, or chicken, they produce volatile basic nitrogen compounds (e.g. ammonia, dimethylamine, trimethylamine) that accumulate in the package headspace[1]. These alkaline metabolites cause a rise in pH and the characteristic off-odors of spoiled meat. The total concentration of these volatile bases, known as total volatile basic nitrogen (TVB-N), is widely used as an indicator of freshness in protein-rich foods[2]. Consequently, monitoring these biochemical changes in real time is essential to ensure food quality and safety.

In recent years, intelligent packaging systems have emerged as an innovative approach for real-time freshness monitoring. Unlike conventional packaging materials that serve primarily as passive barriers, intelligent packaging incorporates active sensing elements that provide real-time information about the condition of the packaged food. One promising strategy involves the use of natural colorimetric indicators capable of responding to chemical changes associated with food spoilage. Among these, anthocyanins have emerged as a premier candidate due to their non-toxicity, biodegradability, and vivid pH-dependent structural transformations. These water-soluble phenolic pigments (e.g. delphinidin derivatives) exhibit different colors at acidic/basic pH, making them useful for sensing spoilage gases (ammonia, amines) and pH increases in food[3,4,5]. This sensitivity makes them ideal for detecting the alkaline environment created by TVB-N accumulation.

For practical application in intelligent packaging, anthocyanins are typically incorporated into biodegradable polymer matrices that form thin indicator films. Biopolymers such as gelatin and cellulose are particularly attractive materials due to their biodegradability, renewability, and excellent film-forming properties. Gelatin, typically available in powdered or granulated form, is a tasteless, odorless biopolymer derived from sources like fish, poultry, bovine, and insects[6]. Its biodegradability, biocompatibility, and ability to form flexible, thin, and translucent films make it suitable for food packaging applications[7,8]. However, neat gelatin films often suffer from high hydrophilicity and poor mechanical integrity. To overcome these limitations, cellulose is incorporated as a reinforcing agent1. Compared to conventional polymers, cellulose offers advantages as a reinforcement in biopolymer composites naturally-sourced from plants, microorganisms, marine species, and agricultural waste[9,10,11].
The high crystallinity and surface area of cellulose provide a synergistic effect, enhancing the thermal stability and mechanical strength of the composite matrix, thereby creating a robust carrier for sensitive indicators.

While various anthocyanin-based films have been reported, a critical gap remains in the systematic comparison of plant sources specifically optimized for a cellulose–gelatin composite matrix. Most existing studies focus on a single pigment source without justifying its selection over others. The novelty of this work lies in the multi-stage optimization process: first, performing a comparative evaluation of three selected plant extracts to identify the extract with the most pronounced and stable pH-responsiveness, and second, integrating this optimized extract into a specifically formulated cellulose–gelatin matrix. This combination is designed to balance rapid ammonia gas diffusion with mechanical durability—a common trade-off in intelligent packaging design.

Therefore, this study sought to evaluate the pH responsiveness of anthocyanins extracted from Hibiscus sabdariffa, Brassica oleracea, and Clitoria ternatea via visible color changes under various pH conditions. The extract that demonstrated the most pronounced pH sensitivity was incorporated into cellulose–gelatin composite films. The resulting films were characterized for their physicochemical and mechanical properties, and their response to volatile ammonia was evaluated to assess their viability as intelligent packaging indicators for monitoring food freshness. It is hypothesized that incorporation of the anthocyanin extract with the most vivid and detectable chromatic transitions into a cellulose–gelatin matrix will produce a stable, pH-responsive indicator film characterized by improved mechanical integrity and distinct colorimetric sensitivity to volatile ammonia gas.

MATERIALS AND METHODS

Materials

H. sabdariffa, C. ternatea, and B. oleracea were outsourced from local farms in Camarines Sur and Agusan del Norte and from a local supermarket at Batangas, Philippines respectively. Gelatin granular powder (CAS No. 9000-70-80), microcrystalline cellulose (CAS No. 9004-34-6), 99.5% v/v food grade ethanol (CAS No. 64-17-5; M.W. 46.07 amu), glycerol, and 32% w/w ammonia solution (CAS No. 1336-21-6; M.W. 35.05 amu) were obtained from Chemline Scientific Corporations., JBL Scientific Inc., and Belman Laboratories. The chemicals used in this study were analytical reagent grade and were used without further purification.

Methods

Extraction of Anthocyanins

Fresh H. sabdariffa calyces, B. oleracea leaves, and C. ternatea flowers were air-dried, powdered, and extracted using 85% ethanol (v/v), with a solid-to-solvent ratio of 1:10 (w/v). The extraction was performed in triplicate using maceration at 5°C for 24 hours. After filtration, the ethanol was removed using a rotary evaporator (Buchi R-300 Dynamic Pro Rotavapor) at 60°C. The concentrated extracts obtained were used for the succeeding analysis7. The percent yield of the extraction can then be calculated using the equation:

$$\%\ Yield = \left(\frac{Actual\ Yield}{Initial\ Amount\ Used}\right) x\ 100 \quad (1)$$

pH Responsiveness of Anthocyanin Extracts

Buffer solutions ranging from pH 1 to 10 were prepared and their respective pH were verified using a pH meter (Mettler Toledo Seven Compact pH Meter S210)[12]. The color response of the anthocyanin extracts was then assessed by mixing the diluted extracts with these buffer solutions13. Color changes were captured using a smartphone camera under consistent lighting conditions and analyzed using an online tool (Print Kick Image Colour Match) for standardized Pantone® matching. The extract showing the best pH responsiveness was further analyzed by recording its absorbance spectrum from 300 to 800 nm using a spectrophotometer (Shimadzu UV-2700). Subsequently, 150 g of the selected plant material was macerated, and the extract was concentrated using a rotary evaporator and freeze-dried using a lyophilizer (Medfuture (USA) MF0–VL10PT Freeze Dryer). The resulting freeze-dried extracts were used for film fabrication.

Confirmatory Tests for Anthocyanins

Standard procedures utilized in the study of Agunos et al.,[14], were used to confirm the presence of anthocyanins in the extract. In the sulfuric acid test, 1 mL of concentrated H SO was added to 2 mL of the extract. An orange color at the interface indicated the presence of anthocyanins. In the sodium hydroxide test, 2 drops of 1 N NaOH were added to 2 mL of the extract. Formation of bluish-green to green color confirmed the presence of anthocyanins.

Preparation of Cellulose-Gelatin-Anthocyanin (CGA) pH-Responsive Films

The CGA composite films were prepared according to the method described by Zhao et al.,[1], with some modifications. Initially, 200 mL solution was prepared by dissolving 6% (w/v) gelatin and 20% (w/w, based on gelatin) glycerol in distilled water at 80 °C, with continuous stirring until complete dissolution. Then, 50% cellulose (w/w, based on gelatin) was mixed into the solution through constant stirring at medium to high speed. Varying quantities of anthocyanin extract were dissolved in water and added to the film-forming solutions: 0, 2%, 4%, and 6% (w/w, based on gelatin), coded as CGA0, CGA2, CGA4, and CGA6, respectively. The final solution was continuously stirred for 30 minutes at room temperature. A total of 45 mL of the film-forming solution was cast onto petri dishes (90 mm × 150 mm), corresponding to a casting area of 63.6 cm^2, to form uniform films. The films were dried in a drying oven (BIOBASE Biologix) at 50 °C for 10 hours. Each formulation was prepared in 3 replicates. After drying, the films were vacuum-sealed and stored in a dark place for further testing.

Analysis of Cellulose-Gelatin-Anthocyanin (CGA) pH-Responsive Films

FTIR Spectroscopy

The FTIR spectra of the developed CGA films with different formulations were determined using the FTIR spectrometer (Shimadzu IRSpirit-X). The spectra were measured by 20 scans per test with a wavenumber range of 4000 cm-1 to 500 cm-1.

Surface Morphology

The surface morphology of the CGA films with different formulations was examined using a JEOL JSM-1500 ITHR/LA Field Emission SEM-EDS. Samples (8×8 mm) were sputter coated with platinum and mounted on aluminum specimen stubs for imaging. Imaging was performed with a working distance of 10 mm, probe current of 25 pA, at 2000× magnification and an acceleration voltage of 3 kV, corresponding to a scale of approximately 10 µm. Environmental conditions during analysis were maintained at 20–23°C and 60–65% relative humidity.

Response of CGA Films to Buffer Solutions pH 1-10

The pH responsiveness of the produced CGA films was tested. The films were cut into square strips (2×2 cm^2), and a few drops of buffer solutions with varying pH levels (1–10) were applied directly onto the film surfaces. After 5 minutes, color measurements were taken using a handheld colorimeter (Linshang LS173 D/8), and the color changes observed were photographed. At each pH level, the total color difference (E) was then calculated 1.

Thickness

Film thickness was determined using a micrometer. Nine random positions on each film along their gauge length were measured, and the average thickness was used for subsequent analyses 1.

Opacity

The developed CGA films were cut into strips measuring 1 cm × 4 cm, placed in the center of a quartz cuvette, and their absorbance was measured using a UV-Vis double monochromator spectrophotometer (Shimadzu UV-2700) at 600 nm with air as reference1. The formula used for calculating the opacity of the films is shown below:

$$\text{Opacity } (mm^{-1}) = \frac{A_{600}}{x} \quad (2)$$

where A600 represents the film's absorbance at a wavelength of 600 nm, and X denotes the thickness of the film (mm).

Water Content and Water Solubility

For the evaluation of water content (WC) and water solubility (WS) of the developed CGA films, the method of Zhou et al.,1, was utilized. First, 2 × 2 cm^2 film samples were prepared, and their initial mass (m) was measured using an analytical balance. The film samples were then oven-dried for 6 hours at 105°C. After drying, the mass of the films (m) was recorded. The water content of the films was calculated using the following equation:

$$\text{WC } (\%) = \frac{m_1 \quad m_2}{m_1} \times 100\% \quad (3)$$

Next, the dried CGA films were submerged for 24 hours in a petri dish containing 15 mL of distilled water at room temperature (25°C). The remaining solid fragments were collected, and the surface water was removed using blotting paper. The films were dried in an oven at 105°C until a constant weight (m3) was achieved. The water solubility of the films was calculated as follows:

$$\text{WS } (\%) = \frac{m_2 - m_3}{m_2} \times 100\% \quad (4)$$

Thermal Stability

The thermal stability of the CGA films was determined using a thermogravimetric analyzer (TA Instruments TGA Q500 V20.13 Build 39). The films with a mass of 10 mg each were mounted in an aluminum pan and subjected to ramp-up heating from 30°C to 600°C. The heating rate was set to 10°C/min under nitrogen gas with a flow rate of 50 cm^3. The mass of each film sample was continuously recorded as the temperature increased. TGA curves were plotted from the data of their percent mass versus temperature.

Mechanical Properties

The mechanical properties of the CGA films, specifically tensile strength and percent elongation at break, were measured in triplicates per formulation using a Shimadzu Autograph AG-IC Universal Testing Machine in accordance with ASTM Standard D882.

Evaluation of pH-Responsiveness of the CGA Films Against Volatile Ammonia

The response of the CGA films to volatile ammonia was determined using the method of Zhou et al.,1, with some modifications. Initially, 80 mL of 0.008 M ammonia solution was prepared and poured into a 250 mL beaker. The films were positioned 1 cm

above the ammonia solution and were enclosed with a watch glass to avoid the escape of volatile ammonia vapor. Subsequently, the sample films were exposed to a standard light source at 25°C, and the a*, b*, and L* values of the films were measured using a colorimeter every 30 minutes for a total of 300 minutes (5 hours).

Data Analysis

All experiments were performed in triplicate (n = 3), and results are expressed as mean ± standard deviation. The data were analyzed for significant differences using a one-way analysis of variance (ANOVA), followed by Tukey's Honestly Significant Difference (HSD) post hoc test to determine specific differences between treatment groups. Statistical significance was defined at a level of = 0.05 ($p < 0.05$). All statistical computations and visualizations were generated using Origin 2025 software.

RESULTS AND DISCUSSION

pH Responsiveness of the Crude Ethanolic Extracts of Selected Plant Samples.

The colorimetric response of the 85% ethanolic extracts of H. sabdariffa calyces, B. oleracea leaves, and C. ternatea flowers across a pH range of 1–10 is presented in Figure 1. Hibiscus sabdariffa (Figure 1A) exhibited limited color stability, transitioning from red to nearly colorless as the pH exceeded 5.0, a behavior consistent with the hydration of anthocyanins into colorless carbinol pseudo-bases. Brassica oleracea (Figure 1B) displayed a broader chromatic range from reddish-pink to yellowish-green; however, a visible loss in color intensity at pH > 7 suggests decreased structural stability in alkaline conditions. In contrast, Clitoria ternatea (Figure 1C) demonstrated the most distinct and stable color transitions, particularly within the pH 6–10 range, which is critical for monitoring meat spoilage typically characterized by a rise in pH5,15,16,17.

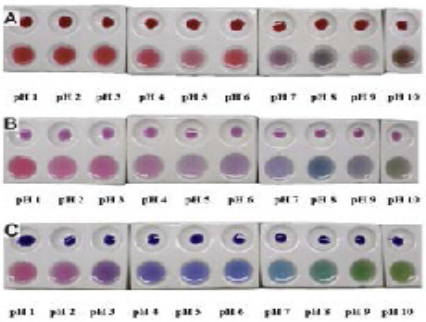

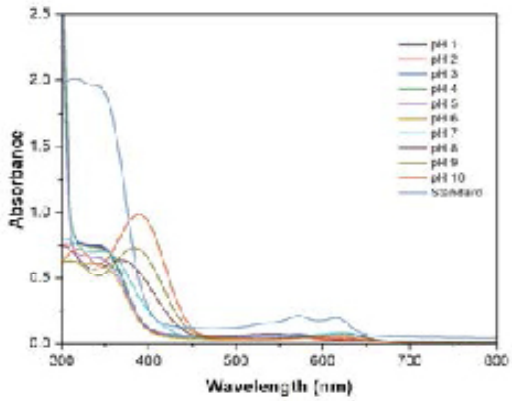

Figure 1. Colorimetric and Spectroscopic Profile of Plant Extracts. (A–C) Visual color response of crude ethanolic extracts in spot plates across pH 1–10 for (A) H. sabdariffa, (B) B. oleracea, and (C) C. ternatea. (D) UV-Vis absorption spectra of C. ternatea extract from 300 to 800 nm, illustrating the quantitative shifts in □max that correlate with the structural transformation of anthocyanins from flavylium cations (acidic) to quinoidal bases (neutral/sub-alkaline) and chalcone anions (alkaline).

UV-Vis spectroscopic analysis of crude C. ternatea extract revealed significant shifts in the absorbance profiles across pH 1-10 (see Figure 1D). At pH 1–3, the extract displays a pink-purple hue corresponding to the dominance of the flavylium cation, with a measured absorption peak (max) at approximately 540 nm. As the pH increases to 4–7, a bathochromic shift (redshift) occurs toward max ~580–620 nm. This quantitative shift reflects the deprotonation of the flavylium cation into neutral and anionic quinoidal bases, which manifest visually as deep blue and purple. At pH 8–9, the spectra flatten in the visible region but maintain broad absorption, resulting in a transitional green appearance. Finally, at pH 10, a sharp hyperchromic effect is observed in the UV-violet region with a distinct peak at max ~390 nm. This signifies the formation of the chalcone anion, which absorbs strongly in the shorter wavelengths, providing the characteristic yellow-green visual output.

Confirmatory Test for Anthocyanin

The confirmatory tests provided qualitative evidence of anthocyanins in the Clitoria ternatea extract, consistent with their known pH-sensitive

behavior. Upon the addition of 1 N NaOH, the extract exhibited a green coloration, indicative of the formation of anthocyanin quinoidal base and chalcone forms under alkaline conditions. Conversely, the introduction of concentrated H SO produced an orange layer at the interface, corresponding to the stabilization of the flavylium cation under strongly acidic conditions. These distinct chromatic shifts are characteristic of anthocyanin pigments and affirm their presence in the extract[14,18].

Percent Yield of the Crude C. ternatea Flower Anthocyanin Extract

The percent yield of the C. ternatea extract obtained from ethanolic extraction was reported as the average yield of 20.06 ± 4.59 %. This amount of yield is lower than the reported yield in the study of Catchillar et al.,19, which could be caused by the ethanol concentration utilized, rotary evaporation parameters (such as duration and temperature), or even the drying procedure.

Physicochemical properties of the developed cellulose-gelatin-anthocyanin (CGA) films using varying formulations

Surface Morphology

The SEM micrograph, depicted in Figure 2, shows that the anthocyanin content and thermal stress significantly influence the surface morphology. The strain and fracture observed in all CGA films could have resulted from thermal stress during rapid drying.

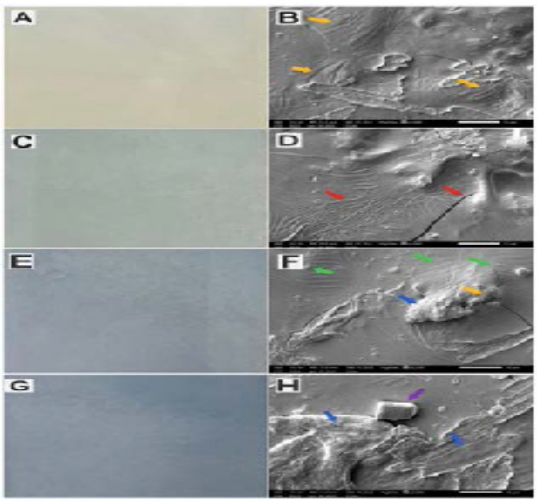

Figure 2. Actual CGA Film and Low Vacuum SEM images of CGA0 (A-B), CGA2 (C-D), CGA4 (E-F), and CGA6 (G-H) at 2000x magnification

The control film (CGA0), containing only cellulose and gelatin, showed a heterogeneous surface with pronounced cracks and regions of delamination. This surface morphology reflects insufficient matrix cohesion, likely due to the absence of stabilizing agents.

The addition of 2% and 4% anthocyanin (CGA2 and CGA4) improved surface morphology significantly, resulting in more uniform, crack-resistant films. Anthocyanins may act as molecular bridges through hydrogen bonding with the hydroxyl and amine groups of cellulose and gelatin, improving matrix cohesion. A similar outcome was reported by Zhou et al.,1, who developed pH-sensitive films from gelatin and cellulose nanofibers infused with anthocyanin (and curcumin). Their anthocyanin-based films exhibited the smoothest and most continuous surfaces, attributed to good miscibility and interactions with the polymer matrix.

At higher loading (6% anthocyanin, CGA6), however, surface morphology deteriorated, showing large aggregates and roughened domains, indicative of anthocyanin crystallization or phase separation. This observation is consistent with the study of Yang et al.,20, in which butterfly pea anthocyanins were loaded into chitosan–gelatin films and observed that higher extract concentrations (≥15%) led to surface roughness, visible particulates, and interfacial cracks due to pigment agglomeration and reduced polymer compatibility.

Likewise, it was observed in fabricated electrospun ethyl cellulose/gelatin nanofiber films incorporated with purple sweet potato anthocyanins that pigment concentrations beyond the optimal level led to surface irregularities, despite initial improvements in matrix homogeneity at low doses21.

Functional Groups

The functional groups present in the CGA films were O–H and C–H stretching linkages and distinct C–O/C–O–C bands (1150–1000 cm^{-1} and ~900 cm^{-1}) imparted by cellulose, amide I, II, III bands (1630 cm^{-1}, 1540 cm^{-1}, and 1350 cm^{-1}) and N–H stretches due to gelatin, and aromatic C=C and phenolic O–H signatures introduced by C. ternatea flower anthocyanins as shown in Figure 3. The varied concentration of anthocyanin extract in CGA films (2%, 4%, 6%) caused a broad O–H/N–H band to shift to higher wavenumbers and

enhanced the intensities of ~1400 cm ¹ and ~920 cm ¹ peaks without generating new peaks beyond those expected from the components. These findings evidence the successful integration of anthocyanins into the cellulose–gelatin network, primarily through intermolecular hydrogen bonding and non-covalent interactions.

This interaction is further substantiated by literature. The incorporation of anthocyanins into biopolymer films leads to enhanced hydrogen bonding, observed as band shifts in the FTIR spectrum, particularly in the O–H region[22]. Similarly, anthocyanin embedded in a bacterial cellulose–gelatin matrix altered the hydrogen bonding environment, producing comparable shifts in the 3200–3300 cm ¹ region1. Moreover, in ethyl cellulose/gelatin films loaded with purple sweet potato anthocyanins, the characteristic phenolic vibrations of anthocyanin were detectable near 1400 and 920 cm ¹, indicating their stable entrapment and interaction with the polymeric matrix[21]. Higher anthocyanin concentration led to more pronounced FTIR peak changes like slight shifts in amide I and II, confirming anthocyanin integration into gelatin-based films by interacting with amide and hydroxyl functional groups without covalent bonding[23].

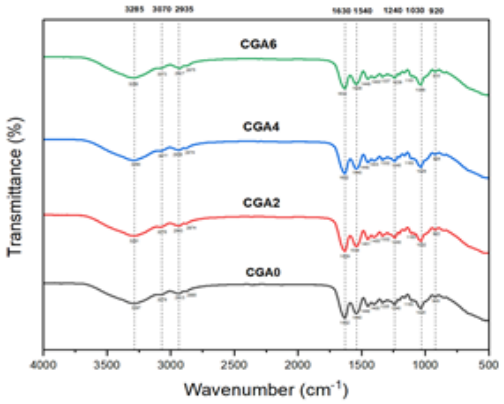

Figure 3. FTIR Spectra of Different CGA Films

pH Responsiveness

The colorimetric performance of the CGA films across the pH 1–10 range is presented in Figure 4. The CGA0 (control) film exhibited negligible color response whereas CGA2 and CGA4 films manifested notable but moderate color change. Among these, CGA6 displayed the most intense and distinguishable colorimetric response, indicating that sensitivity is concentration-dependent.(see Figure 4). The color of the films varies from red-purple to blue to green, from pH 1-10. At acidic pH (1–3), the films exhibit a vibrant red-to-purple hue. This corresponds to the dominance of the flavylium cation. At neutral to sub-alkaline pH (4–7), the films transition to purple and deep blue, matching the original color of the extract. This shift is driven by the deprotonation of the flavylium cation into neutral quinoidal bases, resulting in a bathochromic shift. At alkaline pH (8–10), the films progress to a greenish-blue appearance due to broad absorption[24,25].

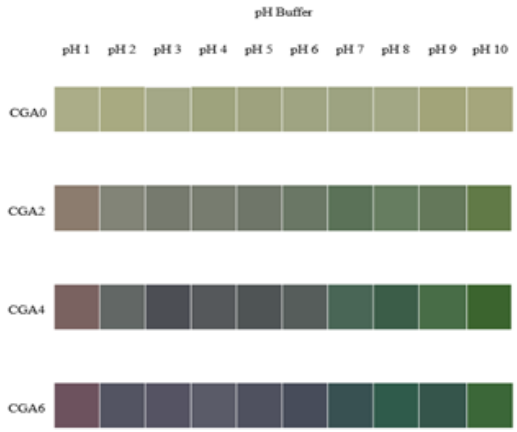

Figure 4. Visible Color Changes of the CGA Films under Different pH Values (pH 1-10)

The films darkened and appeared bluer and greener based on their L*, a*, and b* values (see Table 1). Overall, the films' L* (lightness) and b* (yellow-blue axis) values decreased, while their a* (red-green axis) values increased.

Color

The L* value falls significantly, from 88.44 in CGA0 to 63.08 in CGA6. This indicates that the films darken as the anthocyanin concentration increases. Furthermore, as anthocyanin increases, the a* value becomes increasingly negative, pushing the hue to the green side, while the b* value drops from 8.70 (yellow tone) in CGA0 to -11.79 (blue tone) in CGA6. As anthocyanin concentration increases, E significantly increases from 12.8 to 30.7, indicating a noticeable color change. This observed transition from yellow to blue from CGA0 to CGA6 demonstrates a significant color transformation caused by anthocyanin incorporation.

Table 1. L*, a* and b* values of the CGA Film at Different pH

pH	Parameters	CGA0	CGA2	CGA4	CGA6
		pH Response	pH Response	pH Response	pH Response
1	L*	69.73	53.19	43.82	38.04
	a*	-5.259	4.34	9.71	13.40
	b*	18.87	10.27	4.69	-2.67
	ΔE	4.44	10.49	16.24	19.96
2	L*	68.52	54.69	43.00	35.86
	a*	-5.74	-2.87	-1.86	2.14
	b*	20.87	6.95	0.16	-8.25
	ΔE	4.86	3.99	16.88	17.74
3	L*	67.71	50.51	33.06	35.81
	a*	-5.74	-2.95	0.61	3.65
	b*	16.47	6.20	-4.12	-9.08
	ΔE	3.02	4.46	18.72	15.08
4	L*	65.92	51.20	37.08	38.89
	a*	-6.87	-3.74	-0.65	2.00
	b*	19.55	6.44	-2.24	-7.83
	ΔE	4.67	5.01	15.08	13.13
5	L*	65.55	48.59	35.19	34.56
	a*	-6.13	-4.57	-1.73	1.60
	b*	18.26	6.13	-1.34	-8.62
	ΔE	4.61	8.66	16.01	16.81
6	L*	66.20	48.52	38.71	32.35
	a*	-6.23	-7.75	-3.09	0.38
	b*	16.88	8.00	-0.29	-8.92
	ΔE	3.31	7.95	15.48	16.54
7	L*	65.79	45.51	40.41	32.58
	a*	-6.50	-12.97	-13.72	-9.77
	b*	16.99	11.70	5.46	-3.59
	ΔE	2.05	11.56	14.39	15.72
8	L*	67.34	49.92	36.38	35.09
	a*	-6.15	-12.89	-16.82	-19.33
	b*	17.39	12.86	8.04	4.15
	ΔE	3.52	11.56	19.70	19.89
9	L*	66.36	48.22	42.55	33.37
	a*	-6.34	-12.50	-20.19	-13.97
	b*	22.24	14.03	17.34	1.61
	ΔE	7.75	11.22	23.68	14.03
10	L*	67.10	48.26	38.44	39.45
	a*	-5.30	-16.35	-23.65	-23.70
	b*	21.40	24.684	25.96	21.33
	ΔE	4.67	20.43	32.78	32.45

Note: n = 3

Table 2. Physicochemical Properties of Cellulose-Gelatin-Anthocyanin Films with Varying Quantities of Anthocyanin

Properties	Film			
	CGA0	CGA2	CGA4	CGA6
L*	88.44 ± 1.60a	73.55 ± 2.85b	67.48 ± 1.31c	63.08 ± 1.49d
a*	-2.30 ± 0.22a	-6.42 ± 0.64b	-7.80 ± 0.99b	-6.91 ± 0.69b
b*	8.70 ± 2.32a	-1.25 ± 0.48b	-9.84 ± 0.83c	-11.79 ± 1.73d
E	12.8 ± 1.72a	19.4 ± 2.93b	26.3 ± 1.59c	30.7 ± 1.72d
Color				
Thickness, mm	0.13 ± 0.05a	0.13 ± 0.07a	0.13 ± 0.05a	0.14 ± 0.05a
Opacity, mm-1	10.04 ± 0.01a	11.15 ± 0.01b	12.12 ± 0c	13.31 ± 0d
Water Content, % w/w	7.66 ± 0.1c	9.03 ± 0.41b	9.66 ± 0.15ab	10.12 ± 0.21a
Water Solubility, % w/w	47.99 ± 0.40a	39.55 ± 0.35b	34.88 ± 0.11c	30.60 ± 0.35d

Note: All data were shown as mean ± standard deviation (n = 3) . Data with different letters on the same row indicates significant differences ($p < 0.05$).

Color

The L* value falls significantly, from 88.44 in CGA0 to 63.08 in CGA6. This indicates that the films darken as the anthocyanin concentration increases. Furthermore, as anthocyanin increases, the a* value becomes increasingly negative, pushing the hue to the green side, while the b* value drops from 8.70 (yellow tone) in CGA0 to -11.79 (blue tone) in CGA6. As anthocyanin concentration increases, E significantly increases from 12.8 to 30.7, indicating a noticeable color change. This observed transition from yellow to blue from CGA0 to CGA6 demonstrates a significant color transformation caused by anthocyanin incorporation.

Thickness

The thickness of the CGA0 film was averaged at around 0.13 ± 0.05 mm, CGA2 was around 0.13 ± 0.07 mm, CGA4 was around 0.13 ± 0.05 mm, and CGA6 was around 0.14 ± 0.05 mm. Hence, C. ternatea anthocyanin did not change the overall thickness of the films These results are similar to the findings in the literature7,[26]. This consistency in film thickness is crucial for intelligent food packaging because it enables uniform color distribution, dependable pH responsiveness, and consistent barrier and mechanical qualities. The films' structural stability allows for their practical implementation as visual pH indicators or freshness sensors.

Opacity

The opacity values for CGA0, CGA2, CGA4, and CGA6 were 10.04 mm-1, 11.15 mm-1, 12.12 mm-1, and 13.31 mm-1, respectively. The

increase in opacity can be attributed to stronger interactions between anthocyanins and the film matrix, resulting in a more compact composite structure that restricts light penetration[27,28].

This denser matrix leads to darker and more bluish films at higher anthocyanin levels, consistent with reduced L* values and enhanced opacity. These changes reflect both increased pigmentation and structural compaction, which together enhance the film's light-blocking properties.

Water Content

The water content values for CGA0, CGA2, CGA4, and CGA6 were 7.66 ± 0.10%, 9.03 ± 0.41%, 9.66 ± 0.15%, and 10.12 ± 0.21%, respectively. Water content increased with higher anthocyanin concentrations, likely due to the hydrophilic nature of anthocyanins, which enhance hygroscopicity and disrupt the polymer matrix, allowing greater moisture absorption1,7. Although glycerol can influence water content through hydrogen bonding and increasing affinity for water, its amount was constant across all films, so the observed variation is mainly attributed to anthocyanin concentration[29].

Water Solubility

The water solubility values for CGA0, CGA2, CGA4, and CGA6 were 47.99± 0.4%, 39.55± 0.35%, 34.88 ± 0.11%, and 30.60± 0.35%, respectively. Water solubility decreased as anthocyanin concentration increased, with CGA0 showing the highest solubility and CGA6 the lowest. Although anthocyanins are generally hydrophilic compounds, the observed decrease in solubility of the films with increasing anthocyanin content may be attributed to enhanced intermolecular interactions within the polymer matrix. This reduction may be due to interactions between anthocyanins and the film matrix, such as hydrogen bonding, ϖ-ϖ stacking, electrostatic forces, and decreased availability of free hydroxyl groups, which enhance molecular compatibility and reduce the film's ability to interact with water. The hydroxyl groups present in anthocyanin molecules can form hydrogen bonds with functional groups in gelatin and cellulose, resulting in a more compact and stable polymer network. These interactions reduce the mobility of polymer chains and limit the dissolution of the film when exposed to water. In addition, the reinforcing effect of cellulose may further restrict water penetration into the matrix, thereby contributing to the reduced water solubility observed in the developed films[30,31,32]. Although Azlim et al.,[29], observed an increase in solubility in gelatin films with dragon fruit anthocyanin, this difference may be attributed to variations in polymer composition and anthocyanin source.

Table 3. Characteristic Thermal Degradation Temperatures of CGA Films

Stage of Degradation	Degradation Temperature (°C)
Moisture Evaporation	80-120
Gelatin-Anthocyanin Degradation	200
Cellulose Degradation (1st Tmax)	365
Ashing (2nd Tmax)	402

Thermal Stability

The thermogravimetric analysis of the cellulose–gelatin–anthocyanin films (CGA0, CGA2, CGA4, and CGA6) revealed a consistent three-stage thermal degradation profile across all formulations as depicted in Figure 5. These stages included (1) initial moisture evaporation below 150°C, (2) partial decomposition of gelatin and anthocyanin around ~200°C, and (3) major thermal degradation of the cellulose polymer matrix between 350°C and 450°C. The TGA profile of CGA films is largely dictated by the thermal properties of their individual biopolymer components namely cellulose, gelatin, and anthocyanin.

All films lose a small mass in the low-temperature range, attributed to desorption of adsorbed and bound water. CGA0 typically shows the largest initial mass loss as it contains only the hydrophilic polymer matrix. In contrast, anthocyanin-bearing films (CGA2–CGA6) often lose slightly less mass in this stage. Anthocyanins are polyhydroxy compounds that can bind water, but they also promote additional hydrogen bonding in the matrix, effectively reducing free moisture. Furthermore, gelatin films with anthocyanin microcapsules had a lower moisture content than the control (12.5% vs. 10.4%)[33].

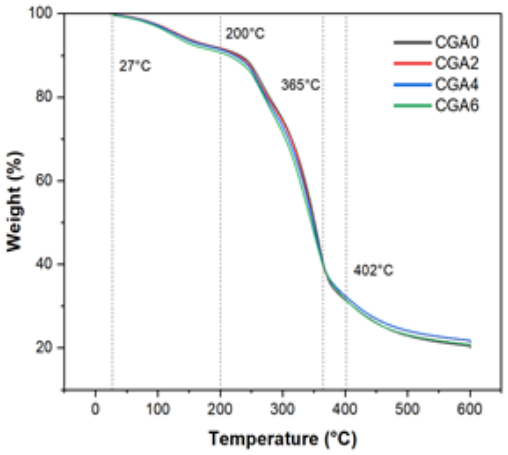

Figure 5. Thermogravimetric Curve of CGA Films of Varying Formulation

The second weight-loss event (~200°C) corresponds to the early breakdown of labile components in the biopolymer matrix such as gelatin chains and low–molecular-weight fractions of anthocyanin accompanied by de-glycosylation, ring opening, and oxidative cleavage. In practice, CGA0 shows a clear inflection or peak near ~200°C. With anthocyanin loading, this degradation tends to shift to slightly higher temperatures. Addition of anthocyanin to a polymer film raised the Tmax of the first degradation stage by 10–30°C as evidenced by higher decomposition temperatures in chitosan/gelatin films with anthocyanin[34,35].

The most pronounced mass loss occurs at high temperatures (350–450°C), reflecting the breakdown of the cellulose backbone and remaining polymer matrix. CGA0 typically exhibits two overlapping peaks: one around ~365°C and another near ~402°C. These likely represent progressive pyrolysis of cellulose. All anthocyanin-loaded films follow a similar pattern, but with notable differences. The onset of this high-temperature degradation is higher in anthocyanin films, and the degradation rate is somewhat slower, indicating enhanced heat resistance. Similarly, anthocyanin–chitosan films exhibit 10–30°C higher decomposition temperatures than pure chitosan films36. This effect is most evident in CGA6, where the highest anthocyanin content leads to a pronounced upward shift in both the second and third degradation stages.

Mechanical properties of the developed CGA films in terms of tensile strength and elongation at break

The tensile strength for CGA0, CGA2, CGA4, and CGA6 were 9.74 ± 5.57 MPa, 8.53 ± 4.67 MPa, 17.83 ± 5.49 MPa, and 21.11 ± 1.48 MPa, respectively. The initial drop in tensile strength from CGA0 to CGA2 is likely caused by early interactions of anthocyanins with the film matrix, which disrupt the hydrogen bonding between cellulose and gelatin, leading to reduced intermolecular cohesion and consequently lower tensile strength. This phenomenon has been reported in polymer composites where the introduction of small amounts of additives initially weakens the matrix before sufficient interactions are established. However, at higher concentrations, anthocyanins reinforce the polymer matrix through strong hydrogen bonding, with tensile strength also influenced by the kind of polymer, source of anthocyanins, and their concentration[37,38]. For CGA4 and CGA6 films, the TS significantly increased, reaching 21.11 MPa. This value is close to several literature benchmarks for anthocyanin-incorporated films, such as gelatin/CMC films (21.98 MPa) and superior over starch-based active films such as starch/chitosan films (3.86 MPa) and starch/MCC (3.21 MPa to 11.18 MPa)39,40,41. Composite cellulose–gelatin films typically exhibit tensile strength values ranging from approximately 5 MPa to over 40 MPa, depending on the type of cellulose used and the cellulose–gelatin ratio. These composite films generally demonstrate improved mechanical strength compared to pure gelatin films due to the formation of a denser molecular network facilitated by hydrogen bonding interactions between cellulose and gelatin chains. The incorporation of anthocyanins may also influence the mechanical properties of the films through additional intermolecular interactions between the hydroxyl groups of anthocyanins and the functional groups of the polymer matrix. The elongation at break (EAB) values for CGA0, CGA2, CGA4, and CGA6 were 0.603%, 0.911%, 1.459%, and 1.789%, respectively. While these values indicate the films remain relatively brittle compared to commercial synthetic plastics like LDPE (EAB > 100%), the increasing trend confirms that anthocyanins exert a dual role. The increasing trend suggests that higher concentrations of C. ternatea anthocyanin enhance film flexibility. This

may be due to a plasticizing effect that reduces intermolecular interactions within the matrix7, as well as the infiltration of anthocyanins into the polymer network, which improves molecular chain mobility42. Additionally, anthocyanins may form hydrogen bonds with amino and hydroxyl groups in the protein matrix, weakening protein–protein interactions and making the film less rigid[29].

Response of CGA films to Volatile Ammonia Vapor

The colorimetric response of CGA films was evaluated through changes in L*, a*, b*, and E during 300 min of exposure to ammonia vapor (136 ppm) at room temperature, with the visual color progression shown in Figure 6. CGA2 exhibited the fastest initial response, reaching E = 4.89 within 90 min and increasing to 13.00 after 300 min, although the color change remained within a dark green range. CGA4 showed a broader and more gradual transition, reaching E = 11.01 at 180 min and 16.01 at 300 min, while CGA6 displayed the slowest onset (E = 2.4 at 90 min) but produced the most pronounced color change, reaching the highest E value (16.43) after 300 min. In contrast, the control film (CGA0) exhibited minimal color variation (E < 3). The differences in response behavior are attributed to anthocyanin concentration, where lower pigment loading enables faster ammonia diffusion but results in less distinct visual changes, while higher pigment content produces stronger but slower color transitions14,30. The color change is caused by ammonia dissolving in the film matrix and generating alkaline species (NH and OH), which induce structural transformations of anthocyanins1. This response simulates the accumulation of volatile basic nitrogen compounds produced during microbial degradation of meat and seafood[43].

During storage, these compounds increase product pH and trigger color changes in pH-sensitive indicators. For example, fish pH has been reported to increase from 5.9 to 7.2 within 48 h at 25 °C during spoilage, accompanied by visible color changes in a chitosan/alizarin film[44].Similarly, anthocyanin-based films showed detectable color differences as TVB-N (total volatile basic nitrogen) levels increased to spoilage thresholds (≈15 mg/100 g) within 36 h of pork storage43. Anthocyanin-based films also responded visibly as TVB-N levels reached higher spoilage thresholds (≈18 mg/100 g) within 72 h of pork storage45. The CGA films exhibited measurable color changes within a few hours of ammonia exposure, indicating high sensitivity to volatile amines associated with early spoilage. These findings support the potential application of CGA films as pH-responsive indicators for monitoring meat freshness in intelligent packaging systems.

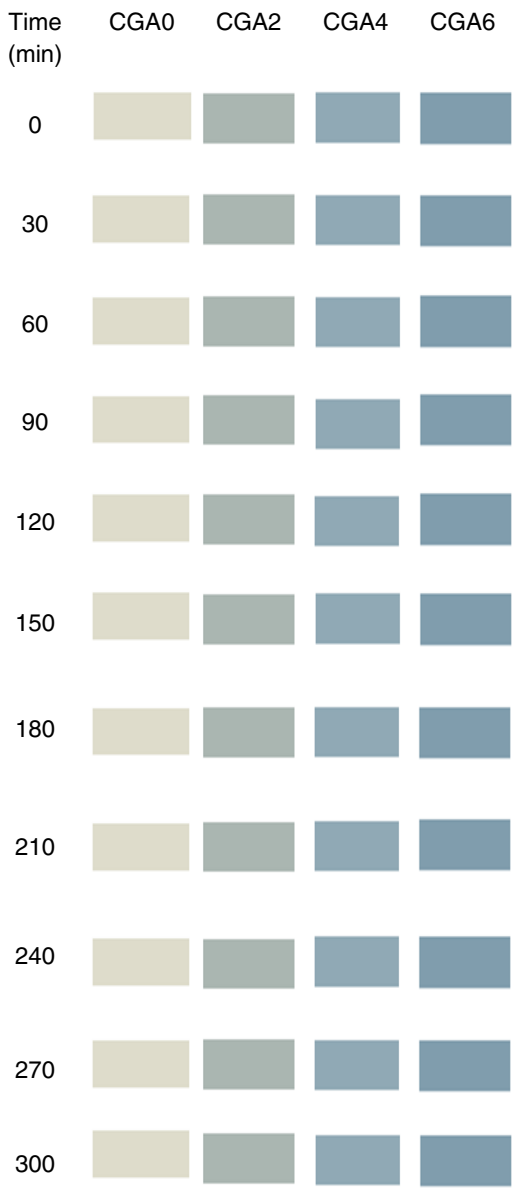

Fig- 6. Visual Color Progression of CGA films during Ammonia Vapor Exposure

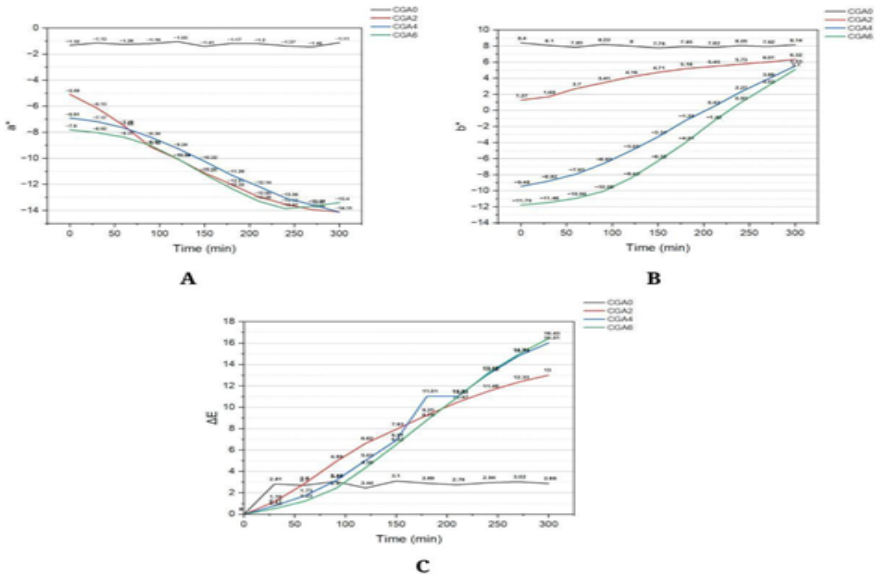

Figure 7. Response of CGA Films to Ammonia Vapor at Varying Times: (A) a* value (red [+] to green [-]), (B) b* value (yellow [+] to blue [-]) and (C) ΔE values (Total Color Difference)

CONCLUSIONS

The ethanolic extract of C. ternatea demostrated distinct color changes and maintained stability across different pH levels. The extraction of C. ternatea reported an average yield of 20.06 ± 4.59%. SEM images revealed that CGA2 exhibited the smoothest surface morphology. FTIR analysis confirmed the presence of hydroxyl, amino, carbonyl, alkyl, and aromatic groups in all CGA films. Among the formulations, CGA6 exhibited the highest pH responsiveness, indicating that increasing anthocyanin concentration enhances color sensitivity of the films. Film thickness remained similar across all samples showing no significant differences ($p > 0.05$). In contrast, CGA4 displayed the highest opacity among the tested formulations. Water content increased with anthocyanin concentration (highest in CGA6, lowest in CGA0), while water solubility decreased accordingly.

Thermal stability and mechanical properties (tensile strength and flexibility) improved with higher anthocyanin levels. Statistical analysis revealed significant differences ($p < 0.05$) in opacity, water content, water solubility, tensile strength, and elongation. Regarding ammonia vapor response, CGA2 reacted fastest but with subtle color change, CGA4 had a moderate and gradual chromatic shift, and CGA6, although slowest, displayed the most vivid and easily distinguishable color change, making it the most effective candidate for visual spoilage detection.

ACKNOWLEDGEMENTS

The authors thank the Batangas State University (BatStateU) - Young LIFTers Program and the Department of Science and Technology Science Education Institute for providing research grants and thesis allowance, respectively. The BatStateU - College of Arts and Sciences Laboratory and the Analytical Research Center for the support and access to laboratory facilities. Technical services from BatStateU Material Testing and Calibration Center, De La Salle Central Instrumentation Facility, Pascual Pharma Corp. Core R&D Laboratory, UP Los Baños College of Agriculture and Food Science Institute of Plant Breeding - Analytical Services Laboratory, and UP Diliman Department of Metallurgy, Mining and Materials Engineering - Materials R&D and Consulting Facility are gratefully acknowledged.

Conflict of interest

The authors declare that they have no known competing financial interests or personal relationships that could have appeared to influence the work reported in this paper.

REFERENCES

1. Zhou, S.; Li, N.; Peng, H.; Yang, X; Lin, D. *Foods*., **2023**, *12*(20), 3719.
2. Zhao, L.; Liu, Y.; Zhao, L.; Wang, Y. *Journal of Agriculture and Food Research*., **2022,** *9*, 100340.
3. Yue, E.; Tuguzbaeva, G.; Chen, X.; Qin, Y.; Li, A.; Sun, X.; Dong, C.; Liu, Y.; Yu, Y.; Zahra, S. M.; Shan, Q.; Jiang, Y.; Du, Z.; Bai, Y. *Phytomedicine: International Journal of Phytotherapy and Phytopharmacology*., **2019,** *56*, 286–294.
4. Roy, S.; Kim, H. C.; Panicker, P. S.; Rhim, J. W.; Kim, J. *Nanomaterials*., **2021**, *11*(4), 877.
5. Gamage, G.C.; Lim, Y.Y.; Choo, W. S., **2021**, *12,* 792303.
6. Said, N.S.; Sarbon, N.M. *Membranes*., **2022**, *12*(5), 442.
7. Rawdkuen, S.; Faseha, A.; Benjakul, S.; Kaewprachu, P. **2020,** *36,* 100603.
8. Shaik, M.I.; Azhari, M.F.; Sarbon, N. M. *Foods*., **2022,** *11*(23), 3797.
9. Ghanayem, H.; Ghanayem, E.; Fathalla, K.; Lela, R. *Animal Health Research Journal*., **2025**, *10*. 144-154.
10. Romruen, O.; Karbowiak, T.; Tongdeesoontorn, W.; Shiekh, K. A.; Rawdkuen, S. *Polymers*., **2022,** *14*(9), 1830.
11. Samrot, A.V.; Ngaakudzwe, K.T.; Rajalakshmi, D.; Prakash, P.; Suresh Kumar, S.; Chandramohan, M.; Alex Anand, D.; Lilly Mercy, J.; Simon, Y.; Saigeetha, S. *Advances in Materials Science and Engineering*., **2022**, 1–13.
12. Reyes, L.F.; Zevallos, L. *Food Chemistry*., **2007**, *100*(3), 885–894.
13. Pramitasari, R.; Gunawicahya, L.N.; Seto, D. *Polymers*., **2022,** *14*(19), 4142–4142.
14. Agunos, R.I.F.; Mendoza, D.V.M.; Rivera, M.A.S. *International Journal of Food Science*., **2020**, 3, 1–7.
15. Sinela, A.; Rawat, N.; Mertz, C.; Achir, N.; Fulcrand, H.; Dornier, M. *Food Chemistry*., **2016**, *214*, 234-241.
16. Abedi-Firoozjah, R.; Yousefi, S.; Heydari, M.; Seyedfatehi, F.; Jafarzadeh, S.; Mohammadi, R.; Rouhi, M.; Garavand, F. *Polymers*., **2022,** *14*(8), 1629.
17. Hasanah, U.; Irnawati, F.; Widyaningrum, R. *Food Research*., **2023**, *7*(1), 131–139.
18. Wiyantoko, D.; Astuti, I. *Indonesian Journal of Chemical Analysis*., **2020**, *3*(1), 22-32.
19. Catchillar, R.P.; Ecalne, J.K.T.; Cayaba, J.M.A.; Aguipo, C.N.P.; Gadian, R.M.R.; Osia, A.K.V.; Saludes, B.O.; Soria, D.J.T.; Torion, R.P.V.S.; Valentin, S.M.; Laguimun, S.E.; Ecalne, J.K.E.T.; Andal, M.S.; Abu-Shendi, S.A.; Catchillar, R.P.; Ecalne, J.K.T.; Cayaba, J.M.A.; Aguipo, C.N.P.; Gadian, R.M.R.; Osia, A.K.V. GSC *Biological and Pharmaceutical Sciences*., **2023**, *23*(2) 142–147.
20. Yang, S.; Ding, Q.; Li, Y.; Han, W. *International Journal of Biological Macromolecules*., **2024**, *259*(1), 129203.
21. Wen, P.; Wu, J.; Wu, J.; Wang, H.; Wu, H. *Foods*., **2024,** *13*(5), 717.
22. Guo, Z.; Zuo, H.; Ling, H.; Yu, Q.; Gou, Q.; Yang, L. *Food Chem*., **2022,** 383, 131915.
23. Daud, A. I.; Latiff, N. F.; Sulaiman, N. F.; Shaik, M. I.; Mohamad, N.J.; Khairul, W. M.; Sarbon, N.M. *Journal of food science*., **2025,** *90*(3), 70134.
24. Mary, S.K.; Aravindhan, R.; Mahadevan, K. *Journal of Food Science and Technology.,* **2020**, *57*(8), 2884–2892.
25. Hidayati, N.A.; Wijaya, M.W.; Bintoro, V.P.; Mulyani, S.; Pratama, Y. *Food Research.,* **2021**, *5*(3), 307–314.
26. Netramai, S.; Kijchavengkul, T.; Kham-Ngam, C.; Sirinupong, P.; Kwanmuang, S.; Samsudin, H.; Lertsiri, S. *The 22nd Food Innovation Asia Conference* **2020** (FIAC 2020)., **2020**, 1-8.
27. Narayanan, G.P.; Radhakrishnan, P.; Baiju, P.; Mubeena S, A. *Food Hydrocolloids for Health*., **2023**, *4*, 100159.
28. Ren, M.; Wang, N.; Lu, Y.; Wang, C. *Foods*., **2025**, *14*(4), 694.
29. Azlim, N. A.; Mohammadi Nafchi, A.; Oladzadabbasabadi, N.; Ariffin, F.; Ghalambor, P.; Jafarzadeh, S.; Al Hassan, A. *Food Science and Nutrition*., **2021,** *10*(2), 597–608.
30. Zhai, X.; Shi, J.; Zou, X.; Wang, S.; Jiang, C.; Zhang, J.; Huang, X.; Zhang, W.; Holmes, M. *Food Hydrocolloids*., **2017,** *69,* 308–317.
31. Mu, L.; Bi, J.; Zhao, H.; Li, J.; Hou, H.; Zhang, G.; Hao, H.; Zhou, L. *Journal of Food Chemistry:* X., **2025,** *28,* 102587.
32. Zeng, F.; Ye, Y.; Liu, J.; Fei, P. *Journal of Food Chemistry: X*., **2023**, *17*, 100531.

33. Leong, C.R.; Daud, N.; Yenn, T.; Cheng, S.; Wen, N.T.; Hamin, N.; Pa'ee, K. *Food Technology and Biotechnology.*, **2021**, *59*, 7069.
34. Rosales-Murillo, S.S.; Sánchez-Bodón, J.; Hernández Olmos, S.L.; Ibarra-Vázquez, M.F.; Guerrero-Ramírez, L.G.; Pérez-Álvarez, L.; Vilas-Vilela, J.L. *Polymers.*, **2024,** *16* (1), 163.
35. Qin, Y.; Tang, Z.; Wang, Y.; Chen, K.; Wang, Z.; Cheng, G.; Chi, H.; Soteyome, T. A. Journal of *Food Chemistry*: X., **2024,** *23,* 10163.
36. Li, L.; Li, Q. *Foods.*, **2025**, *14*(10), 1721.
37. Jiang, G.; Hou, X.; Zeng, X.; Zhang, C.; Wu, H.; Shen, G.; Li, S.; Luo, Q.; Li, M.; Liu, X.; Chen, A.; Wang, Z.; Zhang, Z. *International journal of biological macromolecules.*, **2020,** 143, 359–372.
38. Chen, H.J.; Lee, P.Y.; Chen, C.Y.; Huang, S.L.; Huang, B.W.; Dai, F.J.; Chau, C. F.; Chen, C.S.; Lin, Y.S. *Scientific Repor*ts., **2022**, *12*(1), 10232.
39. Samsi, M.S.; Kamari, A.; Din S,M.; Lazar, G. *Journal of Food Science and Technology.*, **2019,** *56*(6), 3099-3108.
40. Tan, S.X.; Ong, H.C.; Andriyana, A.; Lim, S.; Pang, Y.L.; Kusumo, F.; Ngoh, G.C. *Polymers.*, **2022,** *14*(2), 278.
41. Jeencham, R.; Chiaoketwit, N.; Numpaisal, P.O.; Ruksakulpiwat, Y. *Applied Sciences.,* **2024,** *14*(10), 4242.
42. Yan, J.; Cui, R.; Tang, Z.; Wang, Y.; Wang, H.; Qin, Y.; Yuan, M.; Yuan, M. *Journal of Food Measurement and Characterization.*, **2021**, *15*(5), 3901–3911.
43. Zhang, J.; Shi, J.; Zou, X.; Zhai, X.; Huang, X.; Jiang, C.; Huang, X.; Holmes, M. *Food Chemistry.*, **2019**, *272*, 306–312.
44. Ezati, P.; Rhim, J. *Food Hydrocolloids.*, **2020**, *102*, 105629.
45. Zhang, J.; Huang, X.; Shi, J.; Liu, L.; Zhang, X.; Zhou, X.; Xiao, J.; Zhai, X.; Zhang, D.; Li, Y.; Shen, T. *Food Chemistry.*, **2021**, *355,* 129573.